ARTICLE

Check for updates

Laser cooling of ytterbium-doped silica glass

Esmaeil Mobini[1,2], Saeid Rostami[1], Mostafa Peysokhan[1,2], Alexander Albrecht[1], Stefan Kuhn[3], Sigrun Hein[3], Christian Hupel[3], Johannes Nold[3], Nicoletta Haarlammert[3], Thomas Schreiber[3], Ramona Eberhardt[3], Andreas Tünnermann[3,4], Mansoor Sheik-Bahae[1] & Arash Mafi[1,2 ✉]

Laser cooling of a solid is achieved when a coherent laser illuminates the material in the red tail of its absorption spectrum, and the heat is carried out by anti-Stokes fluorescence of the blue-shifted photons. Solid-state laser cooling has been successfully demonstrated in several materials, including rare-earth-doped crystals and glasses. Here we show the net cooling of high-purity Yb-doped silica glass samples that are fabricated with low impurities to reduce their parasitic background loss for fiber laser applications. The non-radiative decay rate of the excited state in Yb ions is very small in these glasses due to the low level of impurities, resulting in near-unity quantum efficiency. We report the measurement of the cooling efficiency as a function of the laser wavelength, from which the quantum efficiency of the Yb-doped silica is calculated.

[1] Department of Physics & Astronomy, University of New Mexico, Albuquerque, NM 87131, USA. [2] Center for High Technology Materials, University of New Mexico, Albuquerque, NM 87106, USA. [3] Fraunhofer Institute for Applied Optics and Precision Engineering, Albert-Einstein-Str. 7, 07745 Jena, Germany. [4] Institute of Applied Physics, Abbe Center of Photonics, Friedrich-Schiller-Universität, Albert-Einstein-Str. 15, 07745 Jena, Germany. ✉email: mafi@unm.edu

In solid-state laser cooling, anti-Stokes fluorescence removes heat from the material, resulting in net refrigeration. Pringsheim[1] first proposed anti-Stokes fluorescence cooling in 1929 and Epstein et al.[2] reported the first experimental confirmation of solid-state laser cooling in Yb-doped ZBLANP $(ZrF_4-BaF_2-LaF_3-AlF_3-NaF-PbF_2)$ in 1995. Multiple experiments have since confirmed solid-state laser cooling; they have focused on two broad classes of solids: rare-earth-doped (RE-doped) crystals and glasses, and semiconductors. Laser cooling of RE-doped crystals has been the most successful so far[3–5]; the record cooling to 91 K of a 10 mol% Yb-doped YLiF₄ (Yb:YLF) crystal was reported at the University of New Mexico in 2016 (ref. [6]). The only reported laser cooling of semiconductors is that of a CdS nanobelt in 2013 (ref. [7]), but the validity of their results has been questioned recently[8]. Several RE-doped glasses have been successfully cooled[9–15] since the first experimental report by Epstein et al.[2]. However, attempts to cool silica glass, which is arguably the most versatile optical material, have been unsuccessful[16,17] until very recently[18,19]. Here, we report laser cooling of Yb-doped silica glass.

The perennial failure in the laser cooling of RE-doped silica glass made one wonder whether it would ever be possible for the Yb-doped silica glass to have a sufficiently small non-radiative decay rate of the Yb excited-state population to achieve a near-unity internal quantum efficiency. This was examined recently in a spectroscopic study of the Yb-doped silica glass and by looking into the potential decay channels of the Yb excited-state population; it was concluded that there is no a priori reason to reject the possibility of laser cooling for the high-purity Yb-doped silica glass[16]. The background absorption of $5–15\,dB\,km^{-1}$ is commonly achieved in high-purity Yb-doped silica glass used in fiber lasers and amplifiers[17] and is small enough not to be an obstacle to laser cooling. However, it was predicted that for adequate laser cooling, the glass host must be co-doped with modifiers such as Al to mitigate the quenching-induced non-radiative decay for sufficiently high concentrations of Yb ions in silica glass[20,21].

Advancements in solid-state laser cooling may eventually lead to all-optical compact and vibration-free cryocoolers that can reduce the thermal noise in semiconductor-based single-photon detectors or quantum information processing circuits[5]. Another important application is for radiation-balanced fiber lasers (RBFLs), where the cooling from anti-Stokes fluorescence offsets the waste heat generation in the laser[22–27]. RE-doped crystals like Yb:YLF have proven to be the best materials of choice for laser cooling because they have a small inhomogeneous broadening of the absorption lines and a high ion solubility that leads to a higher cooling efficiency[3,5]. RE-doped ZBLAN glass is another successful cooling-grade material, but its low mechanical and chemical stability limits its application for integrated photonics or RBFLs. On the other hand, Yb-doped silica glass is the material of choice for fiber lasers and is commonly used as the substrate in silicon photonics[28–31]. Therefore, potential applications, especially for RBFLs in the near-term and photonic-device cooling in the long-run, are strong motivations for the laser cooling of RE-doped silica glass beside the scientific curiosity.

The primary focus of this paper is to investigate the laser cooling of Yb-doped silica glass. In particular, we will determine the wavelength dependence of the cooling efficiency of our Yb-doped silica glass samples as a function of the pump laser wavelength to observe their transition from the heating to cooling regime.

Results

Determination of the cooling efficiency
The cooling efficiency, η_c, is defined as the net power density (per unit volume) extracted from the material (p_{net}) per unit total absorbed power density (p_{abs}): $\eta_c = {}_{net}/p_{abs}$. The cooling efficiency can be expressed as[5,32] (see Supplementary Note 1 for the derivation)

$$\eta_c(\lambda_p) = \frac{\lambda_p}{\lambda_f}\,\eta_{ext}\,\eta_{abs} - 1, \qquad (1)$$

where λ_f is the mean wavelength of the escaped fluorescence, λ_p is the laser pump wavelength, η_{ext} is the external quantum efficiency, and η_{abs} is the absorption efficiency; they are defined as

$$\eta_{ext} = \frac{\eta_e W_r}{W_{tot}}, \qquad W_{tot} = \eta_e W_r + W_{nr}, \qquad (2)$$

$$\eta_{abs}(\lambda_p) = \frac{\alpha_r(\lambda_p)}{\alpha_r(\lambda_p) + \alpha_b}, \qquad (3)$$

where W_r, W_{nr}, and W_{tot} are radiative, non-radiative, and total decay rates of the excited state, respectively, and η_e is the fluorescence extraction efficiency. α_b is the background absorption coefficient and α_r is the resonant absorption coefficient. In practice, both η_{ext} and η_{abs} must be very close to unity to observe laser cooling, because λ_p cannot be much longer than λ_f to keep $\alpha_r(\lambda_p)$ sufficiently large for a near-unity value of η_{abs}.

It was recently shown by Mobini et al.[16] that it is possible for the Yb excited-state population to have a small non-radiative decay rate in a silica glass host, i.e. $W_{nr} \ll W_r$; therefore, the external quantum efficiency can be near unity. To revisit the arguments presented by Mobini et al.[16], note that the non-radiative decay rate, W_{nr}, can be divided into two separate parts: the multiphonon decay rate (W_{mp}) and the sum of other non-radiative decay rates (W_i) for those channels that are related to the concentration quenching effect, i.e., $W_{nr} = W_{mp} + \Sigma_i W_i$[16,33]. Using the energy-gap law, we showed that the multiphonon decay rate of silica glass is $W_{mp}^{silica} \approx 10^{-8}\,s^{-1}$, while that of ZBLAN is $W_{mp}^{ZBLAN} \approx 10^{-4}\,s^{-1}$; therefore, as far as the multiphoton non-radiative decay rate is concerned, Yb-doped silica glass is a better material than ZBLAN for optical refrigeration[16]. Additional information is provided in Supplementary Note 2.

The non-radiative decay channels related to the concentration quenching are mainly due to the dipole–dipole interactions between Yb ions and impurities, which include OH^-, transition metals, and undesirable RE ions, as well as Yb–Yb interactions in Yb ion clusters. Developing a high-purity Yb-doped silica glass is therefore required to avoid the interactions between the Yb ions and impurities[16]. Additionally, to ensure that Yb ion clustering is suppressed and to further mitigate Yb-impurity interactions, it is imperative for the Yb ion density to remain below the critical ion concentration[33]. It is known that the ion solubility of the silica glass is quite low, i.e., for pure silica glass the critical quenching concentration is $N_c \approx 10^{25}\,m^{-3}$ or lower[34]. However, by using modifiers such as Al and P, the quenching concentration of silica glass can be increased by an order of magnitude[20,21]. To prevent concentration quenching and achieve $\eta_{ext} \approx 1$, it is necessary to keep the Yb ion density below N_c. Quite possibly, this issue has been one of the main reasons behind the previously failed attempts in laser cooling of the Yb-doped silica glass[17]. The Yb-doped silica glass samples that are studied in this paper are all high-purity and are doped with modifiers to increase the Yb ion solubility[35]. The parasitic background absorption (α_b) in these glasses is sufficiently low to ensure that $\eta_{abs} \approx 1$, as is required to achieve laser cooling.

For the laser cooling experiments, we used three different samples of Yb-doped silica glass optical fiber preforms (see "Methods"). We refer to these preforms as sample A, sample B, and sample C, respectively. These preforms are Yb-doped only in the core and their characteristics are listed in Table 1.

Table 1 Properties of the investigated Yb-doped silica glass preforms.

Sample	Codopants	Yb$_2$O$_3$ [mol%]	Yb density [10^{25} m^{-3}]	OH$^-$ conc. [ppm]	Core diam. [mm]	Clad diam. [mm]	Sample length (l) [mm]	α_b (1200 nm) [dB km^{-1}]
A	Al, P	0.12	5.3	3.0	1.7	10.7	28.6	10
B	Al, F	0.10	4.4	1.5	2.6	13.8	28.7	9
C	Al, F, Ce	0.13	5.7	1.5	3.1	14.8	27.8	5
	Error:	±0.01	±0.4	±0.5	±0.1	±0.1	±0.1	±2

The Yb$_2$O$_3$ concentration is measured via electron probe micro-analysis. The Yb density is calculated from the measured Yb$_2$O$_3$ concentration. The given error for the Yb$_2$O$_3$ concentration is related to the uncertainty of the used method in this concentration range. OH$^-$ concentration and parasitic background absorption (α_b) are measured by cut-back method, for which the errors represent the repeatability of the measurement setup.
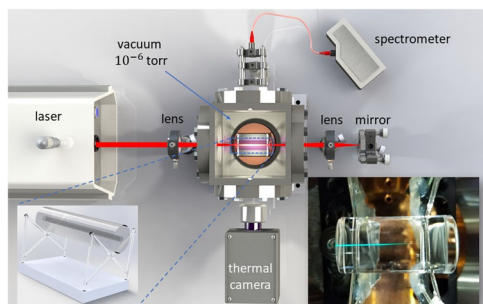

Fig. 1 Schematic of the laser-induced thermal modulation spectroscopy (LITMoS) test setup. A wavelength-tunable continuous wave Ti:Sapphire laser is coupled by a lens of focal length $f = 10$ cm into the Yb-doped silica glass preform through a side window mounted on the vacuum chamber. The transmitted light gets reflected back by a highly reflective mirror and is coupled back into the preform again by another lens of focal length $f = 10$ cm. The lower left inset shows a sketch of the Yb-doped silica glass preform supported by a set of thin silica fibers to minimize the heat load, while the lower right inset shows the actual image of preform supported on the thin silica fibers.
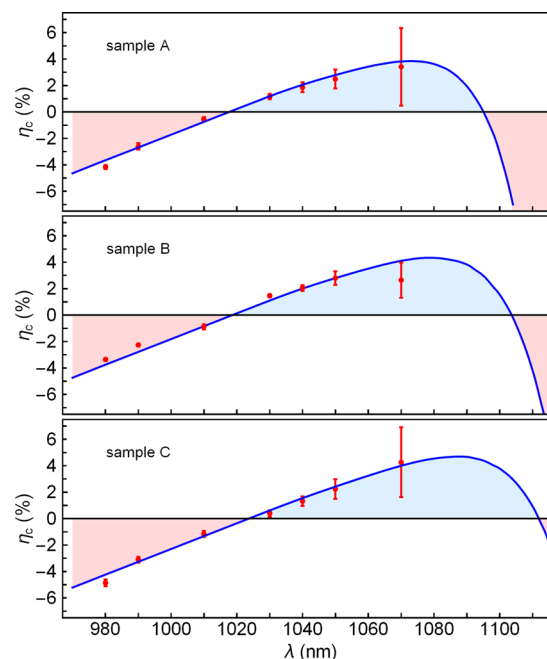

Fig. 2 Measurement of the cooling efficiency. In each subfigure, the red dots with error-bars represent the measured values of the cooling efficiency versus pump laser wavelength for samples A, B, and C, respectively. The blue curved line is a fitting of Eq. (1) to the experimental measurements. The blue-shaded areas represent the net cooling regions and the red-shaded areas represent the net heating regions. The error-bars for cooling efficiency at each pump wavelength are calculated based on the fluctuations in the absorbed pump power and the background thermal radiation.

The background absorption coefficients were measured for large mode-area fibers drawn from the respective preform samples by means of the well known cut-back technique.

To investigate laser cooling and obtain the cooling efficiency, η_c, of the Yb-doped silica glass preforms as a function of the laser pump wavelength, we perform the laser-induced thermal modulation spectroscopy (LITMoS) test on all three samples[5,36] (see Supplementary Notes 3 and 4 for additional information). The LITMoS test setup is shown in Fig. 1. The samples are held by a set of silica fibers inside a vacuum chamber with the pressure of 10^{-6} Torr to minimize the conductive and convective heat-loads on the samples, so the black body radiation remains the only source of heating from the environment. The samples are pumped by a wavelength-tunable continuous wave (CW) Ti-Sapphire laser (980 nm < λ_p < 1070 nm) and the laser light passes through each sample twice using an external mirror.

The spectral features of the samples are captured by a spectrometer through a thermally transparent KCl salt window mounted in the chamber. Similarly, the thermal images are recorded by a thermal camera through the KCl salt window and the images are post-processed to determine the changes in the sample temperatures. To calculate the mean fluorescence wavelength, the samples are initially pumped at $\lambda_p = 1030$ nm. The fluorescence emission then is captured with an optical spectrum analyzer. The calculated mean fluorescence wavelengths of the samples A, B, and C are found to be $\lambda_f^A = 1010$ nm, $\lambda_f^B = 1008$ nm, and $\lambda_f^C = 1008$ nm, respectively[16] (see Supplementary Note 5).

Figure 2 shows the cooling efficiencies as a function of the laser wavelength for the three samples obtained from the LITMoS test. In each subfigure corresponding to the particular sample A, B, or C, the pump laser wavelength is gradually increased; once it becomes longer than approximately the mean fluorescence wavelength, the anti-Stokes fluorescence begins to extract heat from the sample until the cooling efficiency becomes positive, indicating the net laser cooling. As can be seen in Fig. 2, all three samples have been laser cooled. By fitting Eq. (1) to the experimental results and using the values of α_b reported in Table 1, we can find the external quantum efficiency, η_{ext}, of the samples, which are summarized in Table 2. Note that the blue lines in Fig. 2 are the results of the one-parameter fitting—we could have used the fitting procedure to determine the values of α_b as well. However, the lack of experimental data for η_c at wavelengths above 1070 nm results in large uncertainties in α_b; therefore, we have chosen to use the directly measured values in

Table 1, which appear to conform well to our measurements. We note that α_b in Table 1 is measured at 1200 nm wavelength to ensure that the resonant absorption is very small; as such, we are implicitly assuming that α_b does not change significantly down to ~1035 nm wavelength.

Power cooling experiment. The results of the LITMoS tests prove laser cooling in all the Yb-doped silica glass preforms. However, because in the LITMoS test setup, the maximum power of our Ti:Sapphire laser in the cooling wavelength range is less than 900 mW, the signal-to-noise ratio, as can be seen from the error-bars in Fig. 2, is large. Therefore, to enhance and further confirm the laser cooling of our samples, we pumped the preforms with a 10.4 W Nd-doped YLiF$_4$ (Nd:YLF) laser, the wavelength of which at 1053 nm resides in the cooling spectral range of the samples (see Fig. 2). We have shown in Supplementary Note 6 that the optimum wavelength for laser cooling is around 1035 nm in the low absorbance ($\alpha_r l \ll 1$) regime. Our use of the Nd:YLF laser operating at 1053 nm was mainly due to the availability of a high-power source in our laboratory. With multipass pump geometries where $N_p \alpha_r l \gg 1$ (N_p is the number of passes), optimum cooling wavelength will increase in accordance with the maximum cooling efficiencies shown in Fig. 2. Similar to the LITMoS test, the samples were double-pass pumped by the Nd:YLF laser inside the vacuum chamber and the changes of the temperature were recorded by the thermal camera as a function of the exposure time. Figure 3 shows the thermal images of sample A (a) before and (b) after the exposure to the laser light. Figure 3b was taken after the laser was turned on and the sample temperature was stabilized (~40 min). Note that the heat extraction occurs only in the core of each sample, but the entire sample cools almost uniformly in less than a minute. The cooling is easily recognizable by unaided human eye when the thermal camera image become darker after the exposure to the Nd:YLF laser. The bright regions in the thermal image of the sample in Fig. 3 can be misleading; the reason for these bright regions is that silica glass is not transparent in the thermal window and the bright regions on the sample originate from reflections of the thermal radiation

from the side walls of the chamber onto our sample's cylindrical surface and eventually into the thermal camera.

Figure 4 shows the evolution of the temperature of the samples over time while being exposed to the 10.4 W Nd:YLF laser. In each case, the temperature drop can be fitted to the exponential function

$$\Delta T(t) = \Delta T_{max}(e^{-t/\tau_c} - 1), \qquad (4)$$

where we use the following definitions:

$$\Delta T_{max} = \eta_c \frac{P_{abs}}{4\epsilon\sigma T_0^3 A}, \qquad \tau_c = \frac{\rho V c_v}{4\epsilon\sigma T_0^3 A}, \qquad (5)$$

where P_{abs} is the absorbed power, $\epsilon = 0.85$ is the emissivity of the implemented Yb-doped silica glass fiber preforms, $\sigma = 5.67 \times 10^{-8}$ W m^{-2} K^{-4} is the Stefan–Boltzmann constant, T_0 is the ambient temperature, l is the sample length, A is the surface area of the sample, V is the volume of the sample, $\rho = 2.2 \times 10^3$ kg m^{-3} is the silica glass mass density, and $c_v = 741$ J kg^{-1} K^{-1} is the specific heat of the silica glass[37,38].

Equations (4) and (5) can be derived by noting that in the vacuum chamber, the convective and conductive heat transfers are negligible; therefore, the temporal behavior of the temperature obeys the following differential equation[39] (see Supplementary Note 3 for additional information):

$$\rho V c_v \frac{d\Delta T}{dt} \approx -\eta_c P_{abs} - 4\epsilon\sigma A T_0^3 \Delta T, \qquad (6)$$

where the absorbed power in the double-pass experiment is given by

$$P_{abs} = P_{in}\mathcal{T}(1 - e^{-\alpha_r(\lambda_p)l})(1 + \mathcal{T}^2 R_m e^{-\alpha_r(\lambda_p)l}). \qquad (7)$$

$\Delta T = T_s - T_0$, where T_s is the sample temperature. $\alpha_r(\lambda_p)$ is the resonant absorption coefficient of the pump laser. We also have $\mathcal{T} = T_w T_l T_g$, where $T_w = 0.92$ is the transmission of the vacuum chamber windows, $T_l = 0.998$ is the transmission of the lenses, $T_g = 0.96$ is the transmission of the preforms' facets, and
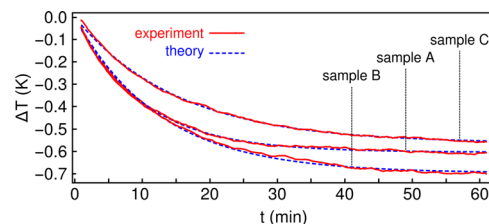
Fig. 4 Temporal cooling behavior of the samples. The temperature changes of the samples A, B, and C are plotted as a function of time, respectively, when exposed to the high-power 1053 nm laser. The ambient temperature was the room temperature of approximately 20 °C. The red lines represent the experimental results and the blue lines represent the fitting of the exponential function in Eq. (4) to the experimental data. The obtained ΔT_{max} and η_{ext} parameters from fitting are presented in Table 2.

Table 2 Results extracted from fitting theory to experimental measurements.

Sample	η_{ext}	ΔT_{max} [K]	τ_c [s]	η_c [%] (1053 nm)
A	0.993 ± 0.003	0.6	599	2.2
B	0.990 ± 0.003	0.7	754	2.7
C	0.984 ± 0.003	0.56	915	2.1

Results of the fitting procedures related to the laser-induced thermal modulation spectroscopy (LITMoS) tests presented in Fig. 2 with Eq. (1), and the temporal evolution curves of the temperature exposed to the high-power 1053 nm laser presented in the power cooling experiment. The errors in η_{ext} signify the range of acceptable values from the fitting of the theoretical curves to the experimental data with error bars in Fig. 2.
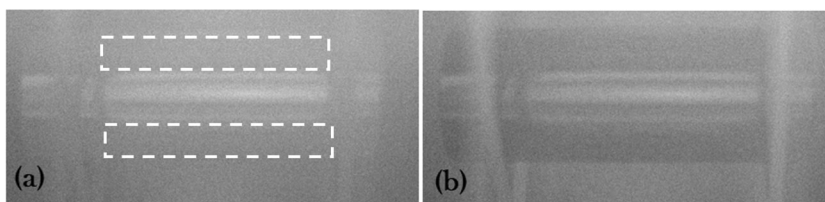

Fig. 3 Thermal camera images before and after cooling. Panel **a** shows the thermal image of samples A before it is exposed to the laser light, and **b** shows its thermal image after nearly 1 h of being cooled by the high-power 105 nm laser. The regions that are used in calculating the temperature changes are marked by the dashed lines in the left column.

$R_{\rm m} = 0.998$ is the reflection of the mirror. Note that the absorption coefficients of samples A, B, and C were measured to be $\alpha_{\rm r}(\lambda_{\rm p}) = 0.43$, 0.52, and 0.50 m^{-1}, respectively. The exponential form presented in Eq. (4) is a direct solution to Eq. (6); by fitting Eq. (4) to the measurements in Fig. 4, the values of the two fitting parameters for each sample, i.e., $\Delta T_{\rm max}$ and $\eta_{\rm ext}$ (via $\tau_{\rm c}$) are extracted and reported in Table 2. We note that the slope of the $\Delta T(t)$ curve at $t = 0$ in Eq. (4) gives us the value of the cooling efficiency at 1053 nm wavelength, i.e., $\eta_{\rm c} = -(\rho V c_{\rm v}/P_{\rm abs})\partial_t \Delta T|_{t=0}$. For each sample, we also calculate the value of $\eta_{\rm c}$ using the two fitted coefficients, and present the results in Table 2; these values all agree well, within the error bars, with the plots of $\eta_{\rm c}$ in Fig. 2 obtained using the LITMoS tests. Video clips of the cooling evolution of the samples are presented in Supplementary Note 7.2.

Discussion

In conclusion, we have demonstrated laser cooling in three separate bulk samples of Yb-doped silica glass optical fiber preform. Each sample has a different Yb ion concentration and each is co-doped with one or more of Al, P, F, and Ce elements. We performed an LITMoS test on each sample and extracted its cooling efficiency and showed that each sample is cooled over a certain laser pump wavelength range. Separately, we exposed each sample to a high-power Nd:YLF laser at 1053 nm wavelength and monitored the temporal evolution of its temperature. The independently extracted cooling efficiencies all agree with those from the LITMoS tests, indicating a maximum cooling of the three samples by 0.6, 0.7, and 0.56 K, respectively, at 1053 nm laser pump wavelength. Because of the geometry of the samples, the temperature variation within each sample is negligible; therefore, the reported temperature drop is nearly uniform in the entire volume of each sample[29]. We emphasize that the added dopants in silica glass results in an increase in the critical quenching concentration of Yb atoms; therefore, the preforms can be sufficiently doped with Yb to observe laser cooling, while keeping the external quantum efficiencies near unity. The experiments allowed us to extract the external quantum efficiency of each sample. We note that this is, to the best of our knowledge, the first reported measurement of the external quantum efficiency of Yb-doped silica glass, the determination of which is critical to laser cooling experiments.

Last but not least, we would like to emphasize that the heat extraction occurs only in the core of each sample. Each sample is surrounded by the undoped (no Yb-doping) silica glass cladding region, which provides a significant thermal load. The cooling in our experiments has been achieved in spite of this large thermal load. We anticipate that in future experiments, we can achieve a larger temperature drop by geometrical optimization[40,41], reducing the thermal load, and using a high-power pump laser at the optimum wavelength for laser cooling at around 1035 nm.

While this paper was under review in another Nature Research journal, we became aware of the successful report of laser cooling of silica fiber by Knall et al.[42], where they report temperature changes up to -50 mK in a fiber with a 21 μm diameter core doped with 2.06 wt% Yb^{3+}, and co-doped with Al$_2$O$_3$ and F$^-$ to increase the critical quenching concentration by a factor of 16 over the largest reported values for the Yb-doped silica.

Methods

Fabrication of silica glass preforms. The high-purity glasses were fabricated by a modified chemical vapor deposition technique. Yb doping was performed by either the all-solution doping technique (sample A)[43] or the gas-phase doping technique (samples B and C)[35]. As stated above, Al codoping was used to ensure a good solubility of the Yb, employing an Al/Yb ratio of greater than 7:1. Codoping with P or Ce, as well as the gas-phase doping technique, reduced the photodarkening loss

of the material (samples B and C). For sample C, a Ce/Yb ratio of about 0.3 was used, which is known to reduce photodarkening substantially[44].

These glasses were developed for single-mode, high-power fiber lasers, so controlling the core-cladding refractive index step was essential; for this reason, codoping with phosphorus[43] or fluorine was used to decrease the refractive index of the material. Fiber lasers using these types of glasses have been used to achieve CW output powers of greater than 4 kW, while maintaining good beam quality[45,46]. Output powers like these can only be accomplished with, among others, high-purity core materials with low background absorption. The background losses of these glasses are listed in Table 1 and are ≤10 dB km^{-1} measured at 1200 nm wavelength. At this wavelength, the main contributions to loss are from Fe^{2+} impurities and Rayleigh scattering. Assuming that Fe^{2+} impurity is the only loss channel, its concentration can be estimated to be around 15 ppb[47]; if scattering losses are also considered, the Fe^{2+} concentration would be even lower. The OH-induced quenching is negligible because the OH concentration in these glasses is very low (see Table 1); similar investigations on Yb-doped aluminosilicate glasses support this[48].

References

1. Pringsheim, P. Zwei bemerkungen über den unterschied von lumineszenz- und temperaturstrahlung. *Z. Phys.* **57**, 739–746 (1929).
2. Epstein, R. I., Buchwald, M. I., Edwards, B. C., Gosnell, T. R. & Mungan, C. E. Observation of laser-induced fluorescent cooling of a solid. *Nature* **377**, 500 (1995).
3. Seletskiy, D. V. et al. Laser cooling of solids to cryogenic temperatures. *Nat. Photonics* **4**, 161 (2010).
4. Nemova, G. & Kashyap, R. Laser cooling of solids. *Rep. Prog. Phys.* **73**, 086501 (2010).
5. Seletskiy, D. V., Epstein, R. & Sheik-Bahae, M. Laser cooling in solids: advances and prospects. *Rep. Prog. Phys.* **79**, 096401 (2016).
6. Melgaard, S. D., Albrecht, A. R., Hehlen, M. P. & Sheik-Bahae, M. Solid-state optical refrigeration to sub-100 kelvin regime. *Sci. Rep.* **6**, 20380 (2016).
7. Zhang, J., Li, D., Chen, R. & Xiong, Q. Laser cooling of a semiconductor by 40 kelvin. *Nature* **493**, 504 (2013).
8. Morozov, Y. V. et al. Can lasers really refrigerate CdS nanobelts? *Nature* **570**, E60 (2019).
9. Gosnell, T. Laser cooling of a solid by 65 K starting from room temperature. *Opt. Lett.* **24**, 1041–1043 (1999).
10. Fernández, J., Mendioroz, A., García, A. J., Balda, R. & Adam, J. L. Anti-Stokes laser-induced internal cooling of Yb^{3+}-doped glasses. *Phys. Rev. B* **62**, 3213–3217 (2000).
11. Hoyt, C. W., Sheik-Bahae, M., Epstein, R. I., Edwards, B. C. & Anderson, J. E. Observation of anti-Stokes fluorescence cooling in thulium-doped glass. *Phys. Rev. Lett.* **85**, 3600–3603 (2000).
12. Thiede, J., Distel, J., Greenfield, S. & Epstein, R. Cooling to 208 K by optical refrigeration. *Appl. Phys. Lett.* **86**, 154107 (2005).
13. Fernández, J., Garcia-Adeva, A. J. & Balda, R. Anti-Stokes laser cooling in bulk erbium-doped materials. *Phys. Rev. Lett.* **97**, 033001 (2006).
14. Nguyen, D. T. et al. Towards all-fiber optical coolers using Tm-doped glass fibers. In (eds. Epstein, R. I., Seletskiy, D. V. & Sheik-Bahae, M.) *Laser Refrigeration of Solids VI [86380G] (Proceedings of SPIE - The International Society for Optical Engineering; Vol. 8638).* https://doi.org/10.1117/12.2002183 (2013).
15. Peysokhan, M., Mobini, E., Allahverdi, A., Abaie, B. & Mafi, A. Characterization of Yb-doped ZBLAN fiber as a platform for radiation-balanced lasers, *Photon. Res.* **8**, 202–210 (2020).
16. Mobini, E., Peysokhan, M., Abaie, B., Hehlen, M. P. & Mafi, A. Spectroscopic investigation of Yb-doped silica glass for solid-state optical refrigeration. *Phys. Rev. Appl.* **11**, 014066 (2019).
17. Knall, J. M. et al. Experimental investigations of spectroscopy and anti-Stokes fluorescence cooling in Yb-doped silicate fibers. In (eds. Epstein, R. I., Seletskiy, D. V. & Sheik-Bahae, M.) *Proc. SPIE 10936, Photonic Heat Engines: Science and Applications* https://doi.org/10.1117/12.2510889 (2019).
18. Mobini, E. et al. Observation of anti-Stokes fluorescence cooling of ytterbium-doped silica glass. *Proc. SPIE 11298, Photonic Heat Engines: Science and Applications II*, **112980G** https://doi.org/10.1117/12.2545233 (2020).
19. Knall, J. M. et al. Experimental observation of cooling in Yb-doped silica fibers. *Proc. SPIE 11298, Photonic Heat Engines: Science and Applications II*, **112980F** https://doi.org/10.1117/12.2548506 (2020).

20. Lægsgaard, J. Dissolution of rare-earth clusters in SiO₂ by Al codoping: a microscopic model. *Phys. Rev. B* **65**, 174114 (2002).

21. Arai, K. et al. Aluminum or phosphorus co-doping effects on the fluorescence and structural properties of neodymium-doped silica glass. *J. Appl. Phys.* **59**, 3430–3436 (1986).

22. Bowman, S. R. Lasers without internal heat generation. *IEEE J. Quant. Electron.* **35**, 115–122 (1999).

23. Nemova, G. & Kashyap, R. Athermal continuous-wave fiber amplifier. *Opt. Commun.* **282**, 2571–2575 (2009).

24. Bowman, S. R., O'Connor, S. P., Biswal, S., Condon, N. J. & Rosenberg, A. Minimizing heat generation in solid-state lasers. *IEEE J. Quant. Electron.* **46**, 1076–1085 (2010).

25. Nemova, G. & Kashyap, R. Radiation-balanced amplifier with two pumps and a single system of ions. *J. Opt. Soc. Am. B* **28**, 2191–2194 (2011).

26. Mobini, E., Peysokhan, M., Abaie, B. & Mafi, A. Thermal modeling, heat mitigation, and radiative cooling for double-clad fiber amplifiers. *J. Opt. Soc. Am. B* **35**, 2484–2493 (2018).

27. Yang, Z., Meng, J., Albrecht, A. R. & Sheik-Bahae, M. Radiation-balanced Yb: YAG disk laser. *Opt. Express* **27**, 1392–1400 (2019).

28. Zhu, X. & Peyghambarian, N. High-power ZBLAN glass fiber lasers: review and prospect. *Adv. Optoelectron* 2010 https://doi.org/10.1155/2010/501956 (2010).

29. Mobini, E., Peysokhan, M. & Mafi, A. Heat mitigation of a core/cladding Yb-doped fiber amplifier using anti-Stokes fluorescence cooling. *J. Opt. Soc. Am. B* **36**, 2167–2177 (2019).

30. Jalali, B. & Fathpour, S. Silicon photonics. *J. Lightwave Technol.* **24**, 4600–4615 (2006).

31. Soref, R. Mid-infrared photonics in silicon and germanium. *Nat. Photonics* **4**, 495 (2010).

32. Sheik-Bahae, M. & Epstein, R. Optical refrigeration. *Nat. Photonics* **1**, 693–699 (2007).

33. Auzel, F., Baldacchini, G., Laversenne, L. & Boulon, G. Radiation trapping and self-quenching analysis in Yb³⁺, Er³⁺, and Ho³⁺ doped Y₂O₃. *Opt. Mater.* **24**, 103–109 (2003).

34. Barua, P., Sekiya, E., Saito, K. & Ikushima, A. Influences of Yb³⁺ ion concentration on the spectroscopic properties of silica glass. *J. Non-Cryst. Solids* **354**, 4760–4764 (2008).

35. Kuhn, S. et al. In *Optical Components and Materials XVI* (eds. Jiang, S. & Digonnet, M. J. F.) Vol. 10914, 15–27 (International Society for Optics and Photonics, SPIE, 2019).

36. Rostami, S., Albrecht, A. R., Volpi, A. & Sheik-Bahae, M. Observation of optical refrigeration in a holmium-doped crystal. *Photonics Res.* **7**, 445–451 (2019).

37. Yoder, P., Vukobratovich, D. & Paquin, R. A. *Opto-Mechanical Systems Design*, 2nd edn (CRC Press, New York, 1992).

38. Karimi, M. Theoretical study of the thermal distribution in Yb-doped double-clad fiber laser by considering different heat sources. *Prog. Electromagn. Res.* **88**, 59–76 (2018).

39. Seletskiy, D. V., Melgaard, S. D., Lieto, A. D., Tonelli, M. & Sheik-Bahae, M. Laser cooling of a semiconductor load to 165 K. *Opt. Express* **18**, 18061–18066 (2010).

40. Nemova, G. & Kashyap, R. Optimization of optical refrigaration in yb3+:yag samples. *J. Luminescence* **164**, 99–104 (2015).

41. Nemova, G. & Kashyap, R. Optimization of the dimensions of an yb3+:zblanp optical fiber sample for laser cooling of solids. *Opt. Lett.* **33**, 2218–2220 (2008).

42. Knall, J. et al. Laser cooling in a silica optical fiber at atmospheric pressure. *Opt. Lett.* **45**, 1092–1095 (2020).

43. Kuhn, S. et al. Modelling the refractive index behavior of Al,P-doped SiO₂, fabricated by means of all-solution doping, in the vicinity of Al:P=1:1. *Opt. Mater. Express* **8**, 1328–1340 (2018).

44. Jetschke, S., Unger, S., Schwuchow, A., Leich, M. & Jäger, M. Role of Ce in Yb/Al laser fibers: prevention of photodarkening and thermal effects. *Opt. Express* **24**, 13009–13022 (2016).

45. Beier, F. et al. Experimental investigations on the TMI thresholds of low-NA Yb-doped single-mode fibers. *Opt. Lett.* **43**, 1291–1294 (2018).

46. Beier, F. et al. Single mode 4.3 kw output power from a diode-pumped Yb-doped fiber amplifier. *Opt. Express* **25**, 14892–14899 (2017).

47. Schultz, P. C. Optical absorption of the transition elements in vitreous silica. *J. Am. Ceramic Soc.* **57**, 309–313 (1974).

48. Kuhn, S. et al. Effect of hydroxyl concentration on Yb³⁺ luminescence properties in a peraluminous lithium-alumino-silicate glass. *Opt. Mater. Express* **5**, 430–440 (2015).

Author contributions

E.M. and A.M. wrote the manuscript and all authors contributed to its final editing. E.M., S.R., and M.P. conducted all the experiments and analyzed the data; A.A. assisted with the Nd:YLF laser setup. S.K., S.H., C.H., J.N., N.H., T.S., and R.E. are responsible for the production and characterization of the silica glass preforms and A.T. supervised their work. A.M. and M.S.-B. led and supervised the laser cooling aspects of the work and participated in the data analysis.

Competing interests

The authors declare no competing interests.

Additional information

Supplementary information is available for this paper at https://doi.org/10.1038/s42005-020-00401-6.

Correspondence and requests for materials should be addressed to A.M.

Reprints and permission information is available at http://www.nature.com/reprints

Publisher's note Springer Nature remains neutral with regard to jurisdictional claims in published maps and institutional affiliations.